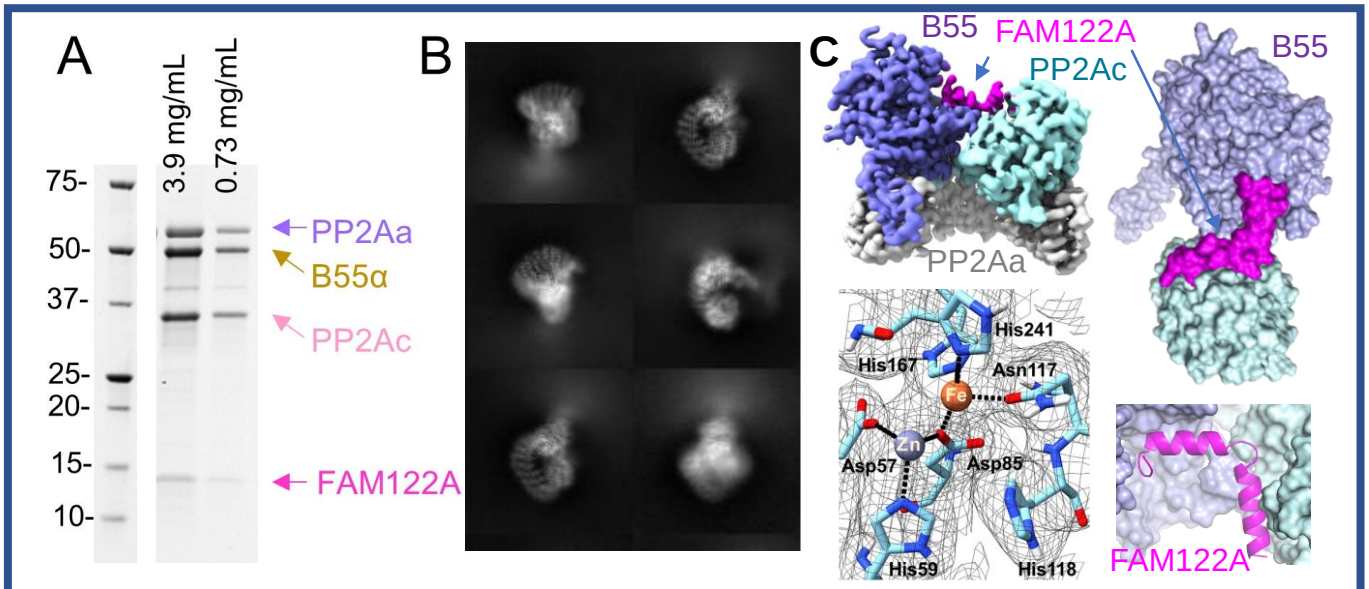

Fig. 1. The PP2A:B55-FAM122A quadruple complex. **A**. SDS-PAGE gel of PP2A:B55 (PP2Aa/PP2Ac/B55; subunits expressed in mammalian or E. coli cells; purified using 4 purification steps) bound to FAM122A (FAM122A stains weakly). **B**. Representative 2D class averages of the final PP2A:B55-FAM122A quadruple complex. **C**. CryoEM map of the consensus 3D refinement (2.55 Å) and figures illustrating the refine structure (including the map at the PP2Ac active site, which had clear evidence for both metals.

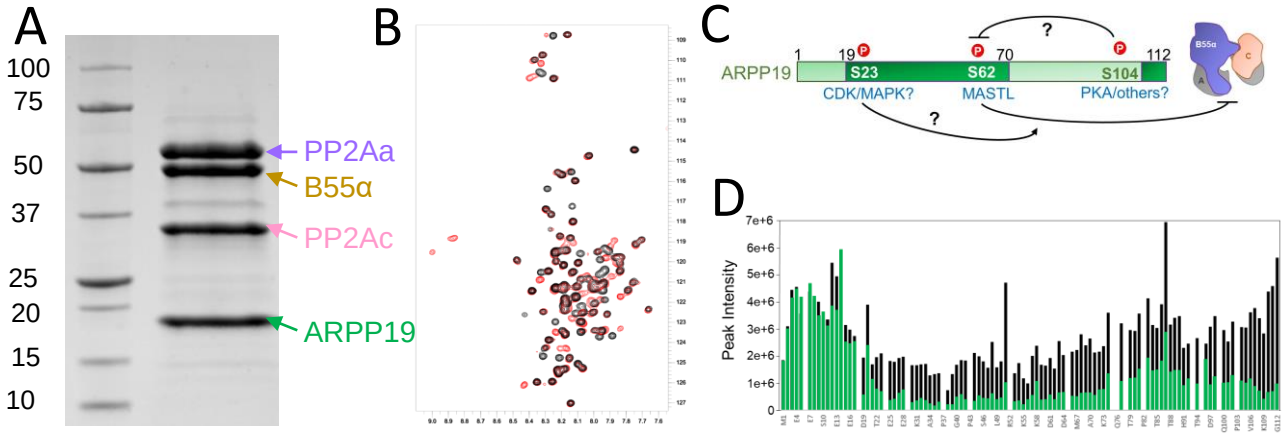

Fig. 2. The PP2A:B55-ARPP19 quadruple complex. **A**. SDS-PAGE gel of PP2A:B55 (PP2Aa/PP2Ac/B55; subunits expressed in mammalian or E. coli cells; purified using 4 purification steps) bound to ARPP19. **B**. Overlay of the 2D [^{1}H,^{15}N] HSQC spectra of ^{15}N-ARPP19 incubated with (red) or without (black) the MASTL kinase, demonstrating S62 is fully phosphorylated. **C**. Domain organization of ARPP19, potential phosphorylation sites and PP2A-triple complex cartoon. **D**. Peak intensity comparison between free ^{15}N-ARPP19 (black) and ^{15}N-ARPP19 bound to the PP2A:B55 triple complex (green). ARPP19 residues 19-112 bind PP2A:B55.

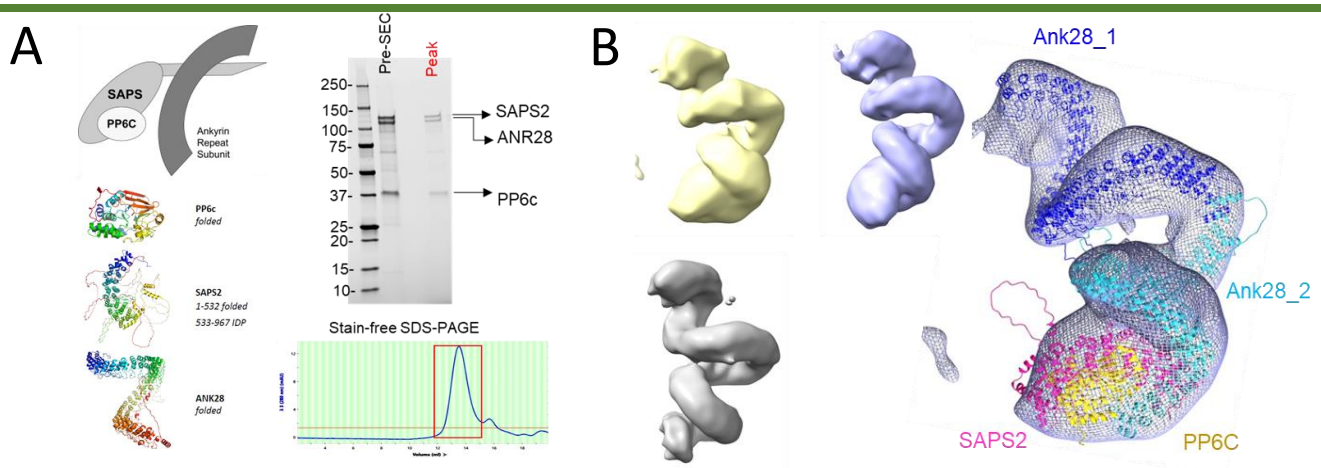

Fig. 3. PP6. **A**. Cartoon depiction of the PP6 triple complex (subunits: SAPS, ANK, PP6C) and alpha fold models for the PP6 subunits. PP6 (expressed in mammalian cells) purified using 4 purification steps, with the last being SEC. **B**. Representative 3D class averages of the PP6 complex Initial rough docking efforts using the alphafold models demonstrates that the ANK subunit clearly dimerizes and that the SAPS2-PP6c complex associates with the end opposite of the ANK dimerization domain. Higher resolution maps are necessary to confidently define how the subunits are organized.